

# Learning from Synthetic Data for Opinion-free Blind Image Quality Assessment in the Wild

Zhihua Wang, Zhi-Ri Tang, Jianguo Zhang, *Senior Member, IEEE*, and Yuming Fang, *Senior Member, IEEE*

**Abstract**—Nowadays, most existing blind image quality assessment (BIQA) models 1) are developed for synthetically-distorted images and often generalize poorly to authentic ones; 2) heavily rely on human ratings, which are prohibitively labor-expensive to collect. Here, we propose an *opinion-free* BIQA method that learns from synthetically-distorted images and multiple agents to assess the perceptual quality of authentically-distorted ones captured in the wild without relying on human labels. Specifically, we first assemble a large number of image pairs from synthetically-distorted images and use a set of full-reference image quality assessment (FR-IQA) models to assign pseudo-binary labels of each pair indicating which image has higher quality as the supervisory signal. We then train a convolutional neural network (CNN)-based BIQA model to rank the perceptual quality, optimized for consistency with the binary labels. Since there exists domain shift between the synthetically- and authentically-distorted images, an unsupervised domain adaptation (UDA) module is introduced to alleviate this issue. Extensive experiments demonstrate the effectiveness of our proposed *opinion-free* BIQA model, yielding state-of-the-art performance in terms of correlation with human opinion scores, as well as gMAD competition. Codes will be made publicly available upon acceptance.

**Index Terms**—Blind image quality assessment, opinion-free, pseudo binary label, unsupervised domain adaptation, gMAD competition.

## I. INTRODUCTION

DIGITAL images have become ubiquitous in almost every aspect of our life. In those tasks from image acquisition, compression, transmission, to storage, etc., there may inevitably exist degradations of image quality, leading to unsatisfactory visual experience [51]. Therefore, it is of great significance to build accurate image quality assessment (IQA) methods to maintain, control, and boost the perceptual quality of images. Based on the accessibility of original reference images, existing IQA methods can be categorized into *full-reference* IQA (FR-IQA) [51], [52], [61], *reduced-reference* IQA (RR-IQA) [50] and *no-reference/blind* IQA (NR-IQA/BIQA) [23], [24], [25], [66]. In the existing literature, it has been demonstrated that FR-IQA methods usually show better generalizability and robustness compared to *blind* IQA (BIQA) models [34].

Zhihua Wang is with the Department of Computer Science, City University of Hong Kong, Hong Kong, also with the Department of Computer Science and Engineering, Southern University of Science and Technology, Shenzhen, China (e-mail: zhihua.wang@my.cityu.edu.hk).

Zhi-Ri Tang is with the School of Physics and Technology, Wuhan University, Wuhan, China (e-mail: GerinTang@163.com).

Jianguo Zhang is with the Department of Computer Science and Engineering, Southern University of Science and Technology, Shenzhen, China (e-mail: zhangjg@sustech.edu.cn).

Yuming Fang is with the School of Information Management, Jiangxi University of Finance and Economics, Nanchang China (e-mail: fa0001ng@e.ntu.edu.sg).

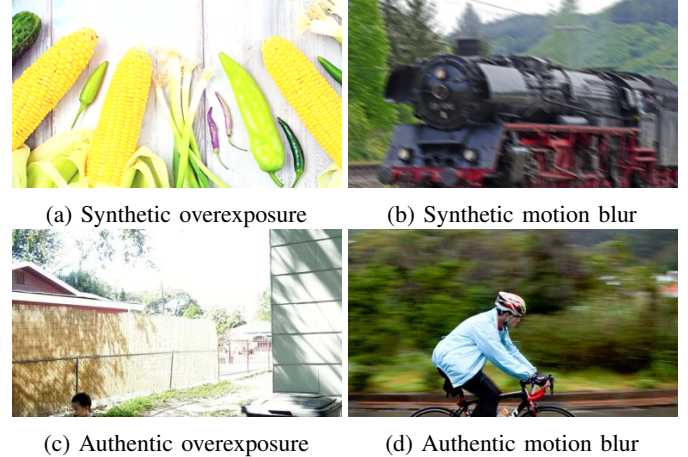


Fig. 1: Representative samples of synthetic distortions from KADID-10k [18] and authentic distortions from KonIQ-10k [12]. (a)-(b) synthetically-distorted images, showing uniformity of distortions. (c)-(d) authentically-distorted images, exhibiting non-uniformity.

However, in many practical settings, reference images are not often available (or may not even exist), thus limiting the use of reference-based IQA methods. Blind IQA (BIQA) models are designed to assess the image quality without the need of reference images.

In principle, BIQA methods first extract features from an image and then map them to a score, indicating its perceptual quality. The key to high performances of BIQA methods lies in the feature representations. Conventional BIQA methods are designed to make use of handcrafted features. Spatially normalized coefficients [28] and codebook-based representations [59] are two examples that have demonstrated impressive performance on common distortion types [39], [22]. Recently, deep neural networks (DNNs) have shown their exceptional capability in the task of automatic learning feature representations, and they have been applied in many BIQA models [24], [10], [65], [23], [34], achieving much better performances on existing IQA benchmarks. However, the successful training of such a model with millions of parameters would require massive quality annotations in the form of mean human-opinion scores (MOSSs), which are largely lacking until now [19] due to the fact that annotating a large-scale IQA image dataset is prohibitively labor-expensive and costly [20] (see TABLE I for a list of datasets). One way to handle this issue is to learn from synthetic data with reliable pseudo labels that can be collected automatically at low cost, instead of

training BIQA models on scored images [20], [58], [25].

Many studies [32], [45] show that by learning from synthetic images, models could achieve supreme performance. Compared to collecting real-world datasets requiring a large number of human annotations, datasets of synthetic images offer several unique advantages. First, collecting a large scale of synthetic images with rich (pseudo) supervisory signals in a lab is much easier and cheaper than annotating a dataset of the same scale captured in the wild. Second, real-world datasets may suffer from the problems of data imbalance and long-tail in distributions; those could be avoided by balancing different categories when synthesizing datasets. In IQA setting, Liu. *et al* [20] explored to generate a large-scale ranked image dataset, where two images in a pair are ranked relatively w.r.t different distortion levels but of the same distortion type. Therefore the *cross-distortion-type* ranking information is absent in this study. Ye. *et al* [58] and Ma. *et al* [25] proposed to train a model using a dataset by including synthetically-distorted images and corresponding pseudo labels predicted by a group of FR-IQA models, achieving excellent performance on synthetic data. Although such methods can also be used for the quality assessment of images captured in the *wild*, they suffer from significant performance decreasing on authentic distortions due to the inevitable *shift* in data distribution between synthetic and real data.

In general, assessing the quality of images degraded by pre-defined *synthetic* distortions, *e.g.*, Gaussian blur, JPEG compression artifacts, JPEG 2000 compression artifacts, Gaussian noise, is much easier than assessing real-world ones. Images captured in the wild are usually distorted by a complex mixtures of *multiple* distortions [8], which are hard to be well-simulated by man-made distortions [6], [8], [12]. Fig. 1 illustrates some representative examples of synthetically- and authentically-distorted images. It could easily observe that synthetic distortions are usually manipulated globally, while authentic ones may be non-uniform [41]. This is a typical example exhibiting the existence of distributional shifts between the simulated and the real-world distortions. Therefore, models trained on synthetic distortions usually perform poorly when generalizing to assess realistic ones. To compensate for the degradation in performance, we need to let knowledge learning from synthetically-distorted domains adapt to authentically-distorted ones. Domain adaptation [7], [40], [43], [44] is a plausible way to alleviate this challenge, which often provides an attractive option where labeled training data are enough but lacking annotations for targeting (test) data. Until now, rare studies discuss it in the setting of IQA.

In this paper, we explore how to learn a deep convolutional neural network (CNN) based *opinion-free* BIQA model for the quality assessment of authentically-distorted images without reliance on any human scores. Technically, we first generate a large number of image pairs, and for each pair, multiple FR-IQA methods (for clarity, we terms them as *agents* in context.) are used to compute pseudo-binary labels indicating which of the two images is of higher quality. We then train a CNN-based model to compute a quality score by fitting these pseudo-binary labels, using a pairwise learning-to-rank (L2R) strategy [2]. It was noted that there are large distributional shifts

between synthetically-distorted images and real-world images degraded by authentic distortions, which seriously hamper the generalization performance of models trained on synthetic data when handling authentic images. To address this challenge, we further introduce unsupervised domain adaptation (UDA) techniques [7], [40], [43], [44] to close the domain gap between synthetic images (source domain) and authentic images (target domain). Specifically, for feature extraction, we design a unit backbone by domain adversarial neural networks to learn discriminative and domain-invariant features by exploiting adversarial learning between a feature extractor and a domain discriminator. In our design, we want the domain discriminator to focus on hard-to-classify examples while assigning less importance to the easy-to-classify ones during training. Here easy-to-classify and hard-to-classify refer to images being easy and hard to distinguish by domain discriminator from synthetically-distorted or authentically-distorted. An adaptive loss is introduced to maneuver this by adding a modulating factor to the cross-entropy loss to put a large weight on hard samples. Moreover, we further explore the usage of domain mixup, which can facilitate a more continuous and linear feature distribution in the latent space with low domain shift, to enhance the performance of adaptive BIQA model .

In summary, our contributions are three-fold. First, a unified learning framework is firstly proposed to learn computational *opinion-free* BIQA models from synthetically-distorted images for the BIQA in the wild without using any human scores, where the supervised signals are rated by a group of FR-IQA models. Second, a simple and easy-to-implement yet effective UDA method, incorporating an adaptive weight loss and domain mixup, to reduce the distributional shift between synthetically-distorted images and the authentically-distorted ones captured in the wild. To the best of our knowledge, our work is the first to exploit adversarial UDA for IQA. Third, extensive experiments on two large-scale realistic IQA datasets demonstrate our proposed method achieves state-of-the-art performance when being evaluated using both human opinion scores as well as gMAD competition.

The rest of this paper is organized as follows. Section II reviews previous works that are closely related to ours. Section III details the algorithm design. Section IV presents the extensive experiment results, and Section V concludes the paper.

## II. RELATED WORKS

In this section, we review previous works that are closely related to ours, including existing approaches to IQA, BIQA in the wild and existing *opinion-free* BIQA models.

### A. Existing Approaches to IQA

long-standing research topic for over 50 years [27]. High quality evaluation mainly pertains to FR-IQA methods, requiring the distorted image along with its pristine counterpart for assessment, *e.g.*, SSIM [51], VSI [61], MAD [16]. However, this kind of method is different from the quality-perceiving of humans, which never requires the information of reference image [49]. Strictly speaking, FR-IQA metrics are the way of

TABLE I: Summary of the characteristics of different public authentically-distorted IQA datasets

dataset	Year	# of distorted images	# of annotations	# of subjects	Score range	Methodology <sup>1</sup>
BID [5]	2011	586	6,446	180	[0, 5]	SS-CQR
CID2013 [46]	2013	480	14,260	188	[0, 100]	ACR-DR
LIVE Challenge [8]	2015	1,162	> 0.35 million	> 8,100	[0, 100]	SS-CQR-CS
KonIQ-10k [12]	2018	10,073	1.2 million	1,459	[1, 5]	SS-ACR-CS
SPAQ [6]	2020	11,125	> 0.16 million	> 600	[0, 100]	SS-CQR

<sup>1</sup> SS: Single stimulus. CQR: Continuous quality rating. ACR: Absolute category rating. CS: Crowdsourcing. DR: Dynamic reference.

evaluating the *fidelity* of distorted images [17]. BIQA models [31], [30], [24] do not rely on the access to reference images for quality evaluation. Early attempts of BIQA reckon on hand-crafted features, *e.g.*, the natural scene statistics (NSS) [29], [31], [28] and Bag-of-Words (BoW) [59], [54]. In recent years, data-driven methods, such as CNN-based BIQAs [1], [24], have outperformed conventional BIQA models based on hand-crafted features in terms of correlation numbers [51] and gMAD competition [21]. However, these methods mainly rely upon large-scale human-rated datasets.

### B. BIQA in the Wild

In recent years, driven by the popularity and advance of portable cameras, mobile phones, as well as photo-centric social Apps, massive authentically-distorted images appear in our lives [6], [8], [30]. Most of these images are captured in the wild by casual, inexpert consumers and are easily distorted by lighting, exposure, noise sensitivity [8]. Normally, authentically-distorted datasets consist of much more diverse contents and complex distortions compared to synthetically-distorted datasets. Frequently used benchmarks guiding the study of authentic distortions include BID [5], CID2013 [46], LIVE Challenge [8], KonIQ-10k [12] and SPAQ [6], where KonIQ-10k and SPAQ are two relative larger datasets each containing more than 10,000 human-scored images.

The majority of existing BIQA models can be used for the evaluation of both synthetic and authentic distortions. Due to the distribution shift between them [66] (see Fig. 1 as an example), models trained on synthetically-distorted images suffer from performance decreasing when generalizing to authentically-distorted ones. For examples, NIQE [30] obtained a performance with correlation numbers reaching to 0.91 on LIVE [38] but only 0.48 on LIVE Challenge [8]. Based on the assumption of Thurstone’s model, Zhang *et al.* [67] proposed a unified L2R framework to train the BIQA model on a combination of synthetic and authentic datasets simultaneously, showing excellent performance on both distortions. Domain adaptation [40], [43], [44] is another potential way to alleviate the influence of distribution shift between synthetic and authentic distortions. In the IQA setting, Chen *et al.* [3] developed the first Maximum Mean Discrepancy (MMD)-based domain adaptation for the quality assessment of screen content images (SCIs). However, different from ours, their methods were supervised and designed for human-rated data; the problem setting of ours is much more challenging.

This is by far the first and only study, to the best of our knowledge, that involves domain adaptation in IQA setting.

### C. Opinion-free BIQA

The annotation process for IQA image datasets requires multiple human scores for each image, and thus the acquisition procedure is extremely labor-intensive and costly (see TABLE I). Developing IQA models without human scores (*i.e.*, *opinion-free* BIQA models) [30] is of great interest. One line for *opinion-free* BIQA is making use of natural scene statistic (NSS) features. Mittal *et al.* [29] proposed the first *opinion-free* BIQA model - TMIQ, where probabilistic latent semantic analysis was applied to characterize quality-aware visual words based on NSS features between pristine and distorted images. Later, Mittal *et al.* [30] introduced NIQE - which is a “completely blind” image quality analyzer without access to any distorted images. NIQE fits the distribution of NSS feature vectors computed from a corpus of pristine image patches with a multivariate Gaussian model (MGV). A Bhattacharyya-like distance between the MVGs of high-quality images and target distorted images was computed as the quality score. Zhang *et al.* [62] further extended NIQE to Integrated Local NIQE (ILNIQE) by incorporating more additional types of quality-aware NSS features and fitting more feature vectors (each patch per MGV) of target distorted image to compute local quality scores on them. They argued that local characteristics could increase the robustness of a BIQA model that is sensitive to local distortion artifacts.

The other line is to learn from pseudo-ground truth, *e.g.*, pseudo-scores [58], pseudo-ranking order [20]. Ye *et al.* [58] proposed blind learning of image quality using synthetic scores (BLISS). Instead of being trained with human-opinion scores, BLISS was trained on synthetic scores derived from FR-IQA measures making use of reciprocal rank fusion (RRF). Wu *et al.* [53] combined the quality values predicted by multiple FR-IQA models according to distortion types since the performance of different FR-IQA models on some specific distortion types may be different from each other. Liu *et al.* [20] presented RankIQA. The supervised signals to train RankIQA is the rank order between images at different distortion levels but with the same distortion type, thus lacking cross-distortion-type ranking information. Ma *et al.* [23] proposed dipIQ, where quality-discriminative image pairs were automatically obtained and labeled by three-trusted FR-IQA models, *i.e.*, MS-SSIM, VIF, and GSMD, achieving excellent performance on synthetically-distorted IQA datasets. To sum up, progress has been made



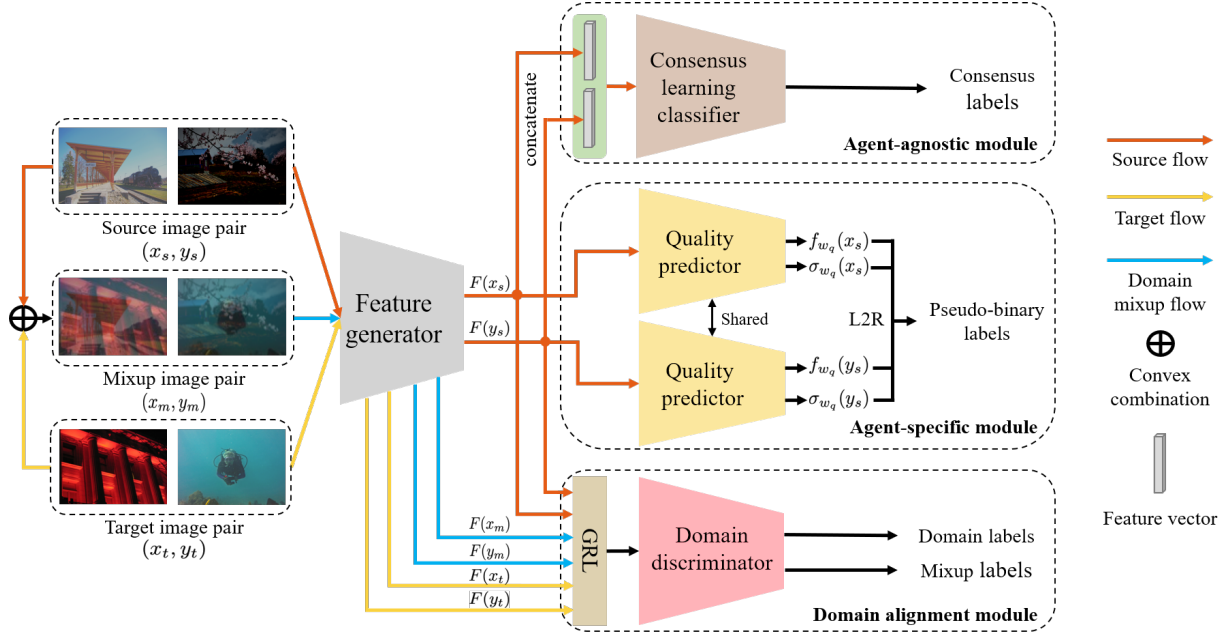


Fig. 2: The overall pipeline of *opinion-free* BIQA model training. The quality predictor takes synthetic image pairs and their corresponding pseudo-binary labels as input to learn a perceptual quality prediction function  $f_{w_q}$ . The domain discriminator tries to reduce the domain shift between synthetic or authentic images. A consensus learning classifier (CLC) provides additional regularization for the rectification of feature extractor. The learned  $f_{w_q}$  is used for the task of image quality predictions in the wild.

on developing *opinion-free* BIQA models, but mainly on *synthetic* IQA scenarios. Few of them can perform satisfactory quality assessment on *authentic* images captured in the *wild*.

### III. METHOD

Our goal is to design a CNN-based BIQA model that is able to learn from an unlabeled synthetically-distorted dataset (source domain)  $\mathcal{X}_s = \{x_s^{(i)}\}_{i=1}^{N_s}$  without using human opinion scores that is of high performance to assess the image quality of authentically-distorted images (target domain)  $\mathcal{X}_t = \{x_t^{(j)}\}_{j=1}^{N_t}$  captured in the wild. Here,  $N_s$  and  $N_t$  are the number of images in  $\mathcal{X}_s$  and  $\mathcal{X}_t$  respectively. Fig. 2 depicts the overall structure of our method. Our unified model contains three modules: agent-specific module, agent-agnostic module, and domain alignment module. In our design, the supervisory signals are from a set of high-performance FR-models [58], [25], [53], termed as *agent* in our context since there are no human opinion scores. It was noted that when assessing the visual quality of an image, those agents agree to disagree, i.e., they have both *consensus* and *specific* information. Thus we introduce an agent-specific and an agent-agnostic module to respectively capture the consensus and specific information from the annotations of a set of high-performance agents of FR-models. The consensus information is captured by a consensus learning classifier (CLC), and module-specific information is implicitly learned by forcing the model to mimic the performance of each agent. Due to the existence of domain shift between synthetically-distorted images and authentically-distorted ones, we further design a domain *alignment* module with a domain discriminator to alleviate this issue. As shown in Fig. 2, we denote the feature

generator, quality predictor, CLC, domain discriminator as  $F$ ,  $Q$ ,  $C$ ,  $D$ , respectively. Since the parameters  $w_f$  of  $F$  are shared among the modules  $Q$ ,  $C$ ,  $D$ , for the sake of clarity, we denoted the union of the parameters of  $F$  and  $Q$  as  $w_q$ , the union of the parameters of  $F$  and  $C$  as  $w_c$ , and the union of the parameters of  $F$  and  $D$  as  $w_d$ , respectively. Then the learned BIQA model can be defined as  $f_{w_q}$ .

#### A. Modules for Quality Prediction

**Agent-specific module:** Given an image  $x_s \in \mathcal{X}_s$ , let  $f(x_s)$  represent its true perceptual quality. We utilize  $M$  full-reference IQA models  $\{f^m\}_{m=1}^M$  (i.e.,  $M$  agents) to estimate  $f(x_s)$ , which are collectively denoted as  $\{f^m(x_s)\}_{m=1}^M$ . It was noted that different agents have different range of predictions, calibrating their outputs will be difficult and unnecessary. Therefore, directly using the output of each agent does not suit directly. To cope with this issue, for an image pair, instead of directly using the predictions of the agents as pseudo labels, we used a rank label inferred based on the outputs by a single agent. In this way, the leaning will focus on the rank of perceptual qualities, rather than an absolute value of the visual quality. Thus for one image pair, in total, we will have  $M$  pseudo-labels, each per agent. Specifically, we first randomly sample  $N$  image pairs  $\{(x_s^{(i)}, y_s^{(i)})\}_{i=1}^N$  from  $\mathcal{X}_s$ . For each image pair  $(x_s, y_s)$ , let  $q_m$  denote its pseudo binary ranking label, with *one* (zero) indicating the perceptual quality of  $x_s$  is ranked *higher* (lower) than  $y_s$  by  $m$ -th agent model, i.e.,  $q_m = 1$  (that is *positive*) if  $f^m(x_s) \geq f^m(y_s)$  and  $q_m = 0$  (that is *negative*) otherwise. In this way, we are able to build a training set of image pairs  $\mathcal{D} = \{(x_s^{(i)}, y_s^{(i)}), q_1^{(i)}, \dots, q_m^{(i)}\}_{i=1}^N$ , where  $x_s, y_s \in \mathcal{X}_s$ .



Since the quality estimates of each agent are noisy and not equally good (or bad) at labeling the input, we introduce two uncertainty variables, *i.e.*, the probabilities of hit rate  $\alpha_m$  and correct reject rate  $\beta_m$  to model the reliability of  $m$ -th agent of IQA annotator, which are denoted in the form of conditional probabilities as:

$$\alpha_m = \Pr(q_m = 1|q = 1) \quad (1)$$

and

$$\beta_m = \Pr(q_m = 0|q = 0), \quad (2)$$

respectively, where  $q = 1$  if  $f(x_s) \geq f(y_s)$  and  $q = 0$  otherwise.

Under the hypothesis of Thurstone's Case V model [42], we make the assumption that the true perceptual quality  $f(x)$  obeys a Gaussian distribution with mean and variance estimated by  $f_{w_q}(x)$  and  $\sigma_{w_q}(x)$ , where  $w_q$  is the model parameter we want to learn. That is to say,  $f_{w_q}(\cdot)$  and  $\sigma_{w_q}(\cdot)$  are two differentiable functions we want to learn for image quality prediction and the corresponding standard deviation (std) (uncertainty) estimation, respectively. Then, the probability of preferring  $x_s$  over  $y_s$  perceptually in an image pair  $(x_s, y_s)$  can be computed from the Gaussian cumulative distribution function  $\Phi(\cdot)$ , which has a close-form as

$$p_{w_q}(x_s, y_s) = \Phi\left(\frac{f_{w_q}(x_s) - f_{w_q}(y_s)}{\sqrt{\sigma_{w_q}^2(x_s) + \sigma_{w_q}^2(y_s)}}\right). \quad (3)$$

During training, the model parameters  $w_q$  along with the uncertainty variables  $\{\alpha, \beta\} = \{\alpha_m, \beta_m\}_{m=1}^M$  are jointly optimized using maximum likelihood function [25], which is defined as follows:

$$\{\hat{w}_q, \hat{\alpha}, \hat{\beta}\} = \underset{w_q, \alpha, \beta}{\operatorname{argmax}} \Pr(\mathcal{D}; w_q, \alpha, \beta), \quad (4)$$

where

$$\Pr(\mathcal{D}; w_q, \alpha, \beta) = \prod_{i=1}^N \left( p_{w_q}(x_s^{(i)}, y_s^{(i)}) \prod_{m=1}^M \Pr(q_m^{(i)}|q = 1) + (1 - p_{w_q}(x_s^{(i)}, y_s^{(i)})) \prod_{m=1}^M \Pr(q_m^{(i)}|q = 0) \right). \quad (5)$$

In practice, we minimize the negative logarithm version of Eq. (4). Therefore, the optimization objective over a min-batch  $\mathcal{B}_s \subset \mathcal{D}$  is equivalently as:

$$\begin{aligned} \ell_q(\mathcal{B}_s; w_q, \alpha, \beta) = \\ -\frac{1}{|\mathcal{B}_s|} \sum_{i=1}^{|\mathcal{B}_s|} \log \Pr(x_s^{(i)}, y_s^{(i)}, \{q_m^{(i)}\}_{m=1}^M; w_q, \alpha, \beta), \end{aligned} \quad (6)$$

where  $|\mathcal{B}_s|$  denotes the cardinality of  $\mathcal{B}_s$ .

**Agent-agnostic module:** To learn the consensus information among the multiple agent annotators, we further add a consensus learning classifier  $C$  as a complementary objective in our pipeline, which can boost final model performance. In another view, the complementary objective could also be considered as a diverse task from quality prediction but highly related to it [4], [35]. Learning the agreement of different agents could improve

the performance of an underlying model [36], [14]. Inspired by this, the supplementary objective is devised as a consensus classification task with the aim of refining feature extractor  $F$  to promote the performance of quality prediction. Technically, the input to CLC is the concatenated feature embeddings of an image pair  $(x_s, y_s) \in \mathcal{D}$ , *i.e.*, the concatenation of  $F(x_s)$  and  $F(y_s)$  (see Fig. 2 for illustration). The supervising signal is generated by the application of majority voting of the pseudo labels, *i.e.*,  $l_c = 1$  if  $\sum_{m=1}^M q_m \geq M/2$  else  $l_c = 0$  otherwise. Other combination implementations, *e.g.*, Bayesian, logistic regression, fuzzy integral and neural network [14] may also be plausible. The loss function of CLC for a mini-batch  $\mathcal{B}_s$  sampled from  $\mathcal{D}$  is defined as follows:

$$\begin{aligned} \ell_c(\mathcal{B}_s; w_c) = -\frac{1}{|\mathcal{B}_s|} \sum_{i=1}^{|\mathcal{B}_s|} \left( l_c g(C(F(x_s^{(i)}) \oplus F(y_s^{(i)}))) \right. \\ \left. + (1 - l_c) g(1 - C(F(x_s^{(i)}) \oplus F(y_s^{(i)}))) \right), \end{aligned} \quad (7)$$

where  $\oplus$  is the feature vector concatenation operation.  $g(x) = (1 - x)^\gamma \log(x)$  is an adaptive loss function (ADL) that can assign high weights on hard-to-classify samples (see Section III-B for detailed definition). Other types of feature vector fusion, *e.g.*, the residual  $F(x_s^{(i)}) - F(y_s^{(i)})$ , the concatenation of feature vectors and their residual  $F(x_s^{(i)}) \oplus F(y_s^{(i)}) \oplus (F(x_s^{(i)}) - F(y_s^{(i)}))$  [1], are also suitable in our setting.

## B. Modules for Domain Alignment

In the wild, images are easily distorted by poor lighting conditions, sensor limitations, lens imperfections, amateur manipulations, and etc. [66]. These distortions are very complex and almost impossible to synthesize in the laboratory [8]. This may cause BIQA models learned only from synthetically-distorted images  $\mathcal{D}$  (source domain) to generalize poorly on authentically-distorted images  $\mathcal{X}_t$  (target domain) [7], [43], [55]. To alleviate this issue, we design a module for domain alignment based UDA to accommodate the features learned from synthetic images to authentic images. This module contains two components: 1) adversarial domain alignment and 2) domain mixup.

**Adversarial domain alignment:** Inspired by the works of generative adversarial learning (GAN) [9] and DANN [7], we introduce an additional domain discriminator  $D$  to distinguish whether an input  $x$  is from the source domain  $\mathcal{X}_s$  or the target domain  $\mathcal{X}_t$  (see Fig. 2 for details). The feature generator  $F$  is trained to produce images in a way that confuses the discriminator, which in turn ensures that the network cannot distinguish between the distributions of  $\mathcal{X}_s$  and  $\mathcal{X}_t$ . Given two samples  $x_s \in \mathcal{X}_s$  with manually assigned domain label  $l_s = 1$  and  $x_t \in \mathcal{X}_t$  with assigned domain label  $l_t = 0$ , the objective function to learn the domain-invariant features is formulated

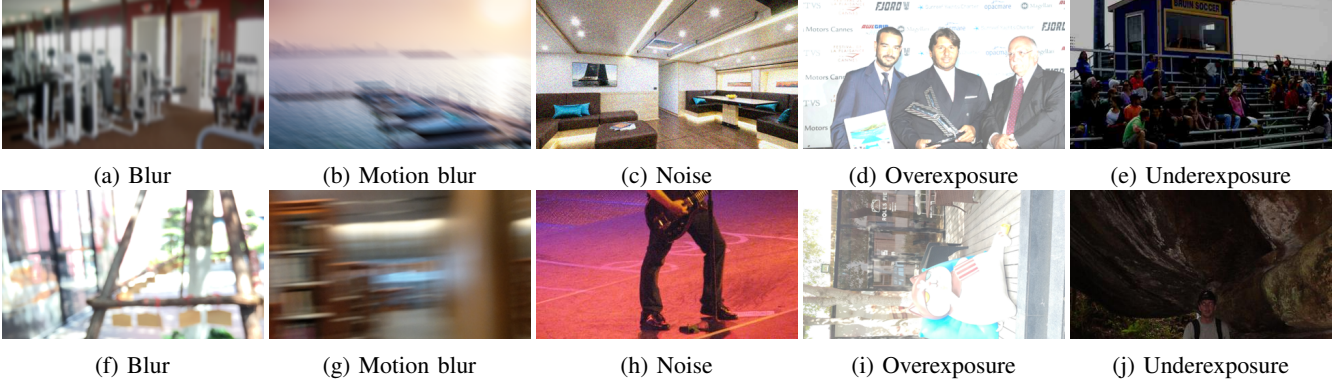


Fig. 3: Representative samples of source domain - synthetically-distorted dataset  $\mathcal{X}_s$  which are generated from Waterloo Exploration Database [22] with man-made distortions, and target domain which are from two authentically-distorted datasets - SPAQ [6] or KonIQ-10k [12]. (a)-(e) are synthetically-distorted images from  $\mathcal{X}_s$ . (f)-(j) are authentically-distorted images from SPAQ or KonIQ-10k, with the same dominant distortion type. For these samples, we can intuitively observe the proximity of the synthetic and authentically distortions.

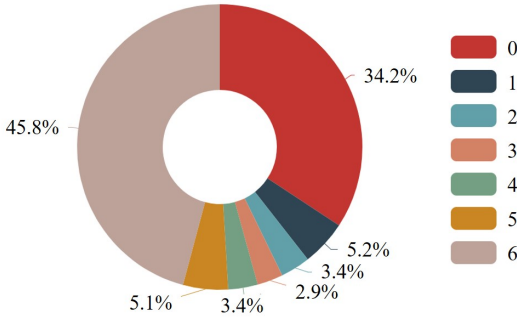


Fig. 4: Percentage of image pairs labeled as *positive* by six FR-IQA agents in  $\mathcal{D}$ . For example, there are 5.1% of image pairs having *five* positive labels, and 34.2% of image pairs having *no* positive labels, etc. In total, roughly 80% of image pairs are in completely agreement with six FR-IQA models (i.e., each pair having six labels all as *positive* or all as *negative*).

as follows by minimizing the cross-entropy loss:

$$\ell_d(\mathcal{X}_s, \mathcal{X}_t; w_d) = - \sum_{i=1}^{N_s} \log(D(F(x_s^{(i)}))) - \sum_{j=1}^{N_t} \log(1 - D(F(x_t^{(j)}))). \quad (8)$$

It was aware that for the samples with small domain shifts, models without UDA might work well, while the transfer performance is likely to be hurt by the samples with large shifts [37]. Therefore, ideally, cross-entropy should assign a non-negligible loss to these easy-to-classify examples (samples with small domain shift) and large ones to hard-to-classify samples (i.e., samples with large domain shifts). To achieve this goal, an ADL is introduced to put larger weights on hard samples than on those easy ones during training. Therefore,

---

#### Algorithm 1: Learning from the synthetic for BIQA in the wild

---

**Input:** A synthetically-distorted image set  $\mathcal{X}_s$  as source domain, an authentically-distorted image set  $\mathcal{X}_t$  as target domain,  $M$  full-reference IQA models  $\{q_m\}_{m=1}^M$ , trade-off hyper-parameters  $\lambda_1$ ,  $\lambda_2$  and  $\lambda_3$ , maximum epochs  $T_1$  for merely training  $f_{w_q}$ , maximum epochs  $T_2$  for domain confusion

**Output:** An optimized BIQA model  $f_{w_q}$

- 1 Pair-wisely sample  $n$  image pairs  $\{(x_s^{(i)}, y_s^{(i)})\}_{i=1}^n$  from  $\mathcal{X}_s$
  - 2 Compute the binary labels  $\{q_m^{(i)}\}_{m=1}^M$  for each pair in  $\{(x_s^{(i)}, y_s^{(i)})\}_{i=1}^n$  to create  $\mathcal{D} = \{(x_s^{(i)}, y_s^{(i)}), q_1^{(i)}, \dots, q_M^{(i)}\}_{i=1}^n$
  - 3 **for**  $t \leftarrow 1$  **to**  $T_1$  **do**
  - 4   | Train  $f_{w_q}$  by minimizing Eq. (6) on  $\mathcal{D}$
  - 5 **end**
  - 6 **for**  $t \leftarrow T_1 + 1$  **to**  $T_1 + T_2$  **do**
  - 7   | Adapt  $f_{w_q}$  to  $\mathcal{X}_t$  by minimizing Eq. (13) on  $\mathcal{D}$  and  $\mathcal{X}_t$
  - 8 **end**
- 

we reformulate Eq. (8) over a mini-batch as follows:

$$\ell_d(\mathcal{B}_s, \mathcal{B}_t; w_d) = - \frac{1}{|\mathcal{B}_s|} \sum_{i=1}^{|\mathcal{B}_s|} g(D(F(x_s^{(i)}))) - \frac{1}{|\mathcal{B}_t|} \sum_{j=1}^{|\mathcal{B}_t|} g(1 - D(F(x_t^{(j)}))), \quad (9)$$

where  $\mathcal{B}_s$  and  $\mathcal{B}_t$  are two min-batches sampled from  $\mathcal{D}$  and  $\mathcal{X}_t$ , respectively.  $g(x) = (1-x)^\gamma \log(x)$  is an ADL applied on  $x$ , and  $\gamma$  controls the weight applied on the samples with large domain shift. Between the feature extractor and domain discriminator, we insert a *gradient reversal layer* (GRL) [7] in the architecture to facilitate the optimization. In the forward pass of the network, the GRL acts as an

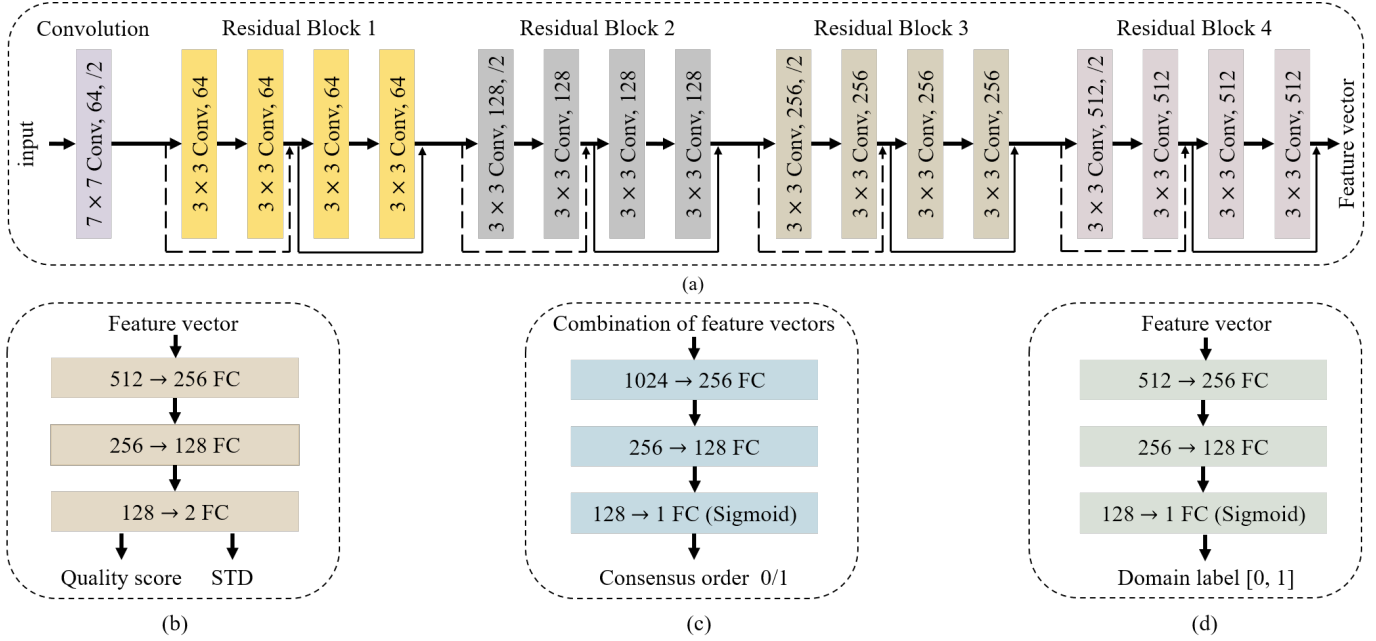


Fig. 5: The detailed architecture of network components with input and output dimensions. **(a)** Feature extractor  $F$ , where the dotted shortcuts increase dimensions. **(b)** Quality predictor  $Q$ , where the outputs are quality score and corresponding STD of image. **(c)** Consensus learning classifier (CLC)  $C$ , where input is combination of feature vectors of image pair. **(d)** Domain discriminator  $D$ .

identity function while reverses the sign of gradients during the backpropagation. In this way, after training, it is hard for the domain discriminator to judge whether the feature of a sample is from the source or target domain (*i.e.*, samples' domain labels are as indistinguishable as possible for the domain classifier), thus resulting in the domain-invariant features.

**Domain mixup:** To further enhance the generalizability and robustness of adaptation models, pixel-level domain mixup [55] is employed to drive the domain discriminator to explore the inter-domain information of two distributions. Let  $x_s \in \mathcal{D}$  and  $x_t \in \mathcal{X}_t$  represent two samples from each domain, and the pixel-level mixup is linearly interpolated to produce a mixup image  $x_m$  and corresponding soft domain labels  $l_m$ :

$$x_m = \lambda x_s + (1 - \lambda)x_t, \quad (10)$$

$$l_m = \lambda l_s + (1 - \lambda)l_t = \lambda, \quad (11)$$

where  $\lambda \in [0, 1]$  is the mixup ratio, and  $\lambda \sim \text{Beta}(\xi, \xi)$ , in which  $\xi$  is set to a constant 2.0 in all experiments. The mixup loss of  $x_m$  is defined as follows:

$$\ell_m(\mathcal{B}_m; w_d) = -\frac{1}{|\mathcal{B}_m|} \sum_{i=1}^{|\mathcal{B}_m|} \left( l_m g(D(F(x_m^{(i)}))) + (1 - l_m) g(1 - D(F(x_m^{(i)}))) \right), \quad (12)$$

where  $\mathcal{B}_m$  is a mixup mini-batch of  $\mathcal{B}_s$  and  $\mathcal{B}_t$ , and  $g(\cdot)$  is the ADL function. Through the introduction of pixel-level mixup, the feature generator can refine the robustness and generalization ability of  $f_{w_q}$ , especially when there exists distribution oscillation in the test phase [55].

### C. Joint Learning and Adaptation

In the training phase, the final joint optimization objective function can be written as:

$$\ell(\mathcal{B}_s, \mathcal{B}_t, \mathcal{B}_m) = \ell_q(\mathcal{B}_s) + \lambda_1 \ell_c(\mathcal{B}_s) + \lambda_2 \ell_d(\mathcal{B}_s, \mathcal{B}_t) + \lambda_3 \ell_m(\mathcal{B}_m), \quad (13)$$

where  $\lambda_1$ ,  $\lambda_2$  and  $\lambda_3$  are hyperparameters that control the trade-offs between quality assessment learning and domain adaptation. Stochastic gradient descent (SGD) is used to update the network parameter vectors  $\{w_q, w_d, w_c, \alpha, \beta\}$ . In the test phase, the learned feature extractor and quality predictor are used for the final assessment of input images.

## IV. EXPERIMENT AND RESULTS

To demonstrate the efficacy of our method, a set of experiments are conducted. We first describe the experimental details and then present the extensive experiment results. Our results show that our proposed method can learn a state-of-the-art *opinion-free* BIQA model for image quality prediction in the wild.

### A. Datasets

Four datasets are used in our experiment to test the performance of the proposed method, including Waterloo Exploration Database [22] to construct  $\mathcal{X}_s$  as the source domain, two large-scale authentically-distorted datasets - KonIQ-10k [12] and SPAQ [6] behaving as  $\mathcal{X}_t$  for domain adaptation and performance evaluation, and a newly established authentically-distorted dataset, including more than 100K images, as gMAD playground for the test of generalizability.



TABLE II: Correlations between model predictions and MOSs on LIVE [39] (a synthetic IQA dataset as reference), KonIQ-10k [12] and SPAQ [6], respectively. In each sub-table, top, middle, and bottom sections list performances of three knowledge-driven, three DNN-based, and our proposed *opinion-free* BIQA models, respectively. Ours( $\mathcal{X}_t$ ) with different  $\mathcal{X}_t$  indicates our methods being applied to different target domain, and *naïve* means no target domain. The top two correlations obtained by BIQA models are highlighted in boldface

SRCC	LIVE[39]	KonIQ-10k[12]	SPAQ[6]
QAC [56]	0.868	0.092	0.340
NIQE [30]	0.906	0.530	0.703
ILNIQE [62]	0.898	0.506	0.714
RankIQA <sup>1</sup> [20]	0.898	0.483	0.584
dipIQ [23]	<b>0.938</b>	0.236	0.385
Ma19 [25]	0.919	0.456	0.379
Ours(naïve)	0.856	0.634	0.807
Ours(KonIQ-10k)	0.907	<b>0.717</b>	<b>0.826</b>
Ours(SPAQ)	<b>0.920</b>	<b>0.712</b>	<b>0.838</b>

PLCC	LIVE	KonIQ-10k	SPAQ
QAC	0.863	0.244	0.371
NIQE	0.904	0.538	0.712
ILNIQE	0.903	0.531	0.721
RankIQA	0.892	0.482	0.587
dipIQ	<b>0.935</b>	0.435	0.497
Ma19	<b>0.917</b>	0.462	0.391
Ours(naïve)	0.849	0.652	0.813
Ours(KonIQ-10k)	0.906	<b>0.740</b>	<b>0.831</b>
Ours(SPAQ)	0.912	<b>0.736</b>	<b>0.844</b>

<sup>1</sup> <https://github.com/YunanZhu/Pytorch-TestRankIQA>.

**Waterloo Exploration Dataset [22]:** This dataset consists of 4,744 high-quality natural images collected from the Internet, with a large span of visual content diversity. It was mainly used for testing the generalizability of IQA models, *e.g.*, P-test, L-test, D-test, as well as gMAD competition [22], [21]. Liu *et al.* [20] and Ma *et al.* [25] simulated synthetically-distorted datasets based on the pristine images to train CNN-based BIQA models. Here, we also make use of the Waterloo dataset for generating  $\mathcal{X}_s$ .

**KonIQ-10K [12]:** It is one of the largest IQA datasets consisting of 10,073 quality scored images in the wild selected from 10 million YFCC100m entries, presenting a broad range of diverse contents and authentic distortions. A total of 1.2 million of reliable human ratings were obtained through crowdsourcing with 1,459 crowd workers. As a result, each image has approximately 120 quality scores.

**SPAQ [6]:** This dataset was constructed by Fang *et al.*, the largest to date smartphone photograph dataset (as named SPAQ). It consists of 11,125 images captured by 66 smartphones. Most of the images were captured by unprofessional photographers, where the capturing processes are easily affected by realistic camera distortions, *e.g.*, lighting conditions, sensor limitations, lens imperfections. These artifacts are hard to be simulated by synthetic distortions. The human ratings are collected

from a large subjective experiment conducted in a laboratory environment, where each image has about 15 human ratings. **Dataset for gMAD in the wild:** In order to test the generalizability of our proposed methods, we further collect a *large-scale authentically*-distorted image dataset<sup>1</sup> as the candidate pool for gMAD competition. Specifically, we first downloaded 750K images from Flickr<sup>2</sup> with diverse real-world distortions. The near-duplicate images were then removed by the command-line tool `imgdupes()`<sup>3</sup>, and those images of pure texts were also deleted, such as ppt, book pages, using OCR tool (`pytesseract`)<sup>4</sup>, and the images without Image Maker (*e.g.*, Canon, Nikon, etc.) were de-duplicated. This resulted in a dataset of 635K naturally distorted photographic images. Afterwards, following the protocol in [47], we sampled 100K images uniformly *w.r.t.*, image attribute scores, *i.e.*, bit-rate, JPEG compression ratio, brightness, colorfulness, contrast, and sharpness. Finally, the images were down-sampled to a maximum width or height of 1,024 as a way to further reduce possible visible artifacts. It is worth noting that this new dataset presents a *wide* range of realistic distortions, such as sensor noise contamination, blurring (out-of-focus, motion), underexposure, overexposure, contrast reduction, color deviation, and a mixture of multiple distortions above, thus serving a good platform to deploy the gMAD competition to test the generalizability of our models.

## B. Construction of $\mathcal{D}$

1) *Synthesizing authentic distortions:* As mentioned before, we simulate the source training set  $\mathcal{X}_s$  by taking each image from Waterloo Exploration Dataset [22] as a reference. As discussed by Ghadiyaram *et al.* [8], the authentic distortions could be seen as a mixture of several degradations in an unknown order that are inherently caused during image acquisition, processing, transmission, storage, etc. (see Fig. 3). Therefore, the way to simulating the authentic distortions is of vital importance. After careful observations, it was found that out-of-focus, motion blur, compression artifacts, sensor noise, overexposure, underexposure, vignetting, and color changes are the dominating distortions in several existing authentically-distorted IQA datasets, *e.g.*, LIVE Challenge [8], KonIQ-10k [13] and SPAQ [6]. Based on this fact, we include ten types of synthetic distortions with five levels of severity to simulate the authentic distortions, *i.e.*, Gaussian blur (simulate out-of-focus), motion blur, JPEG compression (simulate compression artifacts), JP2K compression (simulate compression artifacts), Gaussian noise (simulate sensor noise), overexposure, underexposure, vignetting, chromatic aberration (simulate color changes) and contrast decrements (simulate color changes). We deform each pristine image in four ways, *i.e.*, with (1) a single distortion, (1) random combination of two distortions, (3) random combination of three distortions, and (4) random combination of four distortions, where the distortion order is random excluding (1). We yield a total of  $4744 \times 50 = 273,200$  images, *i.e.*,  $n_s = 273,200$  (the proportions of four categories

<sup>1</sup> <https://mega.nz/folder/G5ox0AoD#QCykopZV1De6NSAE0334gQ>

<sup>2</sup> <https://www.flickr.com/photos/tags/flicker/>

<sup>3</sup> <https://github.com/knjcode/imgdupes#against-large-dataset>

<sup>4</sup> <https://pypi.org/project/pytesseract/>

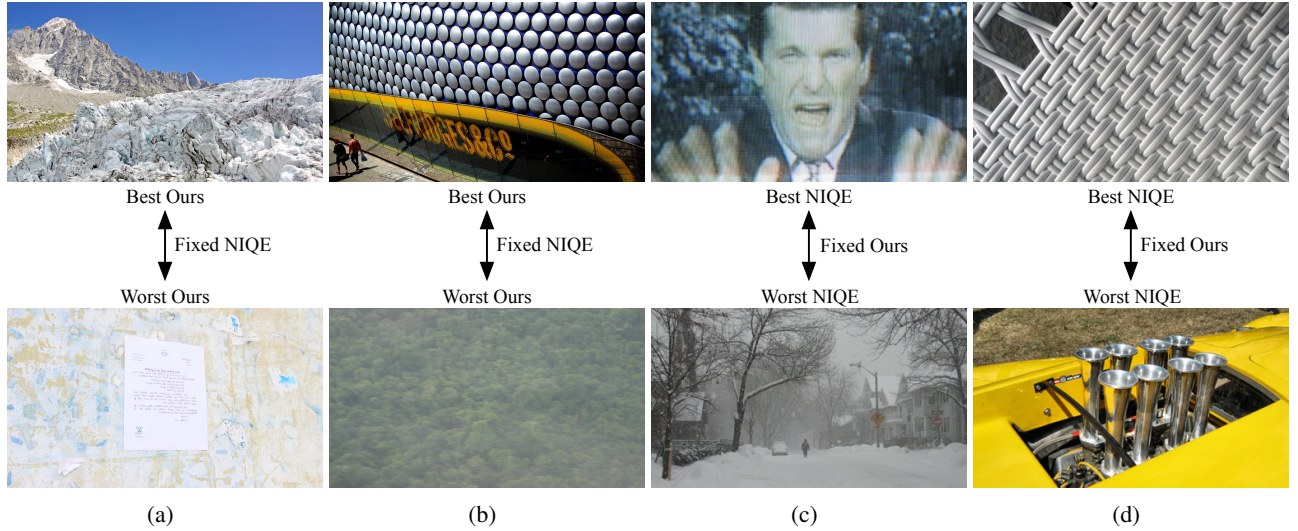


Fig. 6: Representative gMAD pairs between our method and NIQE when  $\mathcal{X}_t$  is KonIQ-10k [12]. (a) Fixing NIQE at the low quality level. (b) Fixing NIQE at the high quality level. (c) Fixing ours at the low quality level. (d) Fixing ours at the high quality level.

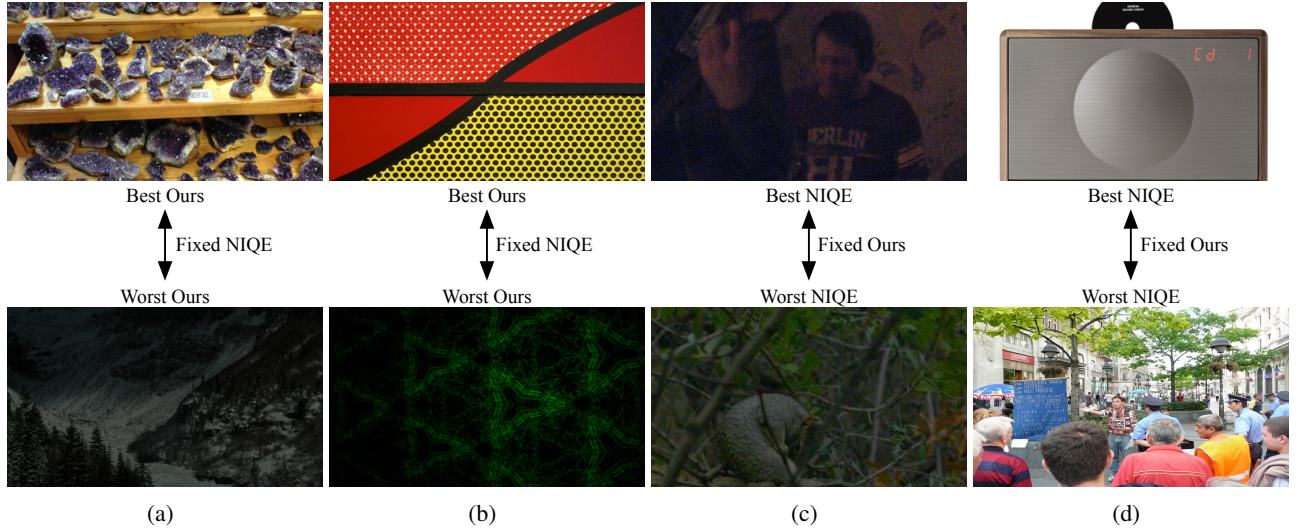


Fig. 7: Representative gMAD pairs between our method and NIQE when  $\mathcal{X}_t$  is SPAQ [6]. (a) Fixing NIQE at the low quality level. (b) Fixing NIQE at the high quality level. (c) Fixing ours at the low quality level. (d) Fixing ours at the high quality level.

are 40%, 30%, 20%, and 10%, respectively) Fig. 3 illustrates representative simulated images and authentically degraded images with similar distortion types. From those images, we could observe that the simulated distortions are perceptually similar to the corresponding authentic ones.

2) *Generating pseudo binary labels:* For a fair comparison, we randomly generate four types of image pairs  $(x, y)$ , following the same protocol in [25]. Specifically, the two images in a pair present (1) different distortion levels of the same distortion types applied to the same reference image; (2) different distortion types and levels, but applied to the same reference; (3) different distortion types, levels and references; (4) one distorted and the other undistorted, both from the same reference image. After distortion, we generate about 426,684 image pairs, *i.e.*,  $n = 426,684$  (the proportions of four categories are about 11%, 49%, 28%, and 12%, respectively).

We use six state-of-the-art FR-IQA models as agents without training on human-rated IQA datasets to assign the pseudo-binary labels to each pairs in  $\mathcal{D}$ , *i.e.*, FSIM<sub>c</sub> [63], SR-SIM [60], NLPD [15], VSI [61], MDSI [33] and GMSD [57], due to their excellent performance. Implementations of all six models were obtained from the respective authors' released codes with default parameters. To test the consensus of all six FR-IQA models, we report the annotation consistency on  $\mathcal{D}$  in Fig. 4. We can easily conclude that approximately 80% of image pairs are in agreement with all models, indicating the rationality and reliability of these FR-IQA models in the quality assessment of synthetically-distorted images.



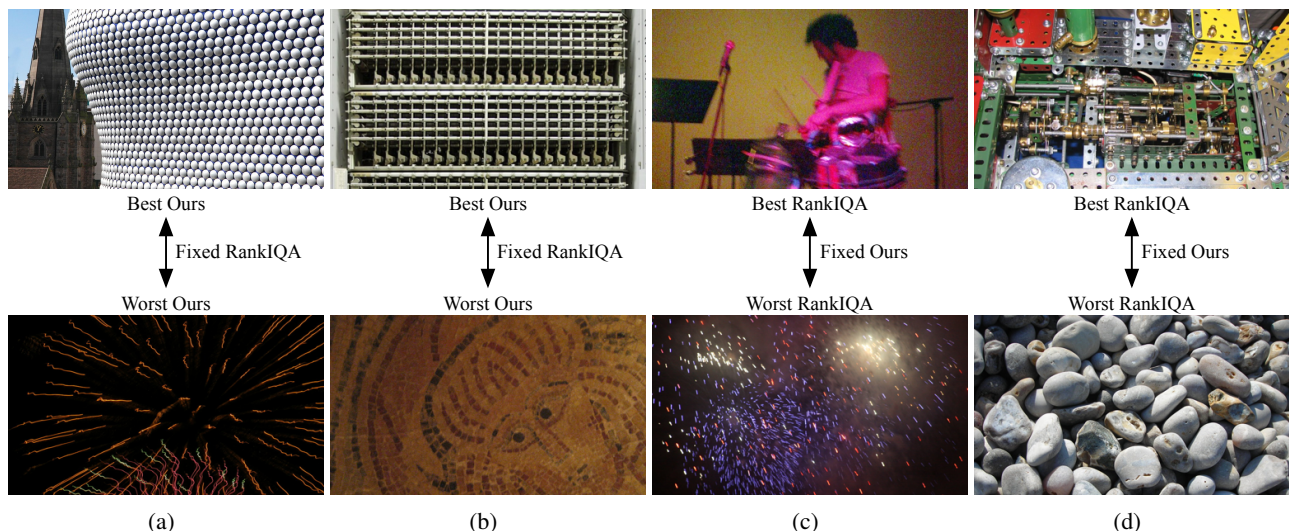


Fig. 8: Representative gMAD pairs between ours and RankIQa [20] when  $\mathcal{X}_t$  is KonIQ-10k [12]. (a) Fixing RankIQa at the low quality level. (b) Fixing RankIQa at the high quality level. (c) Fixing ours at the low quality level. (d) Fixing ours at the high quality level.

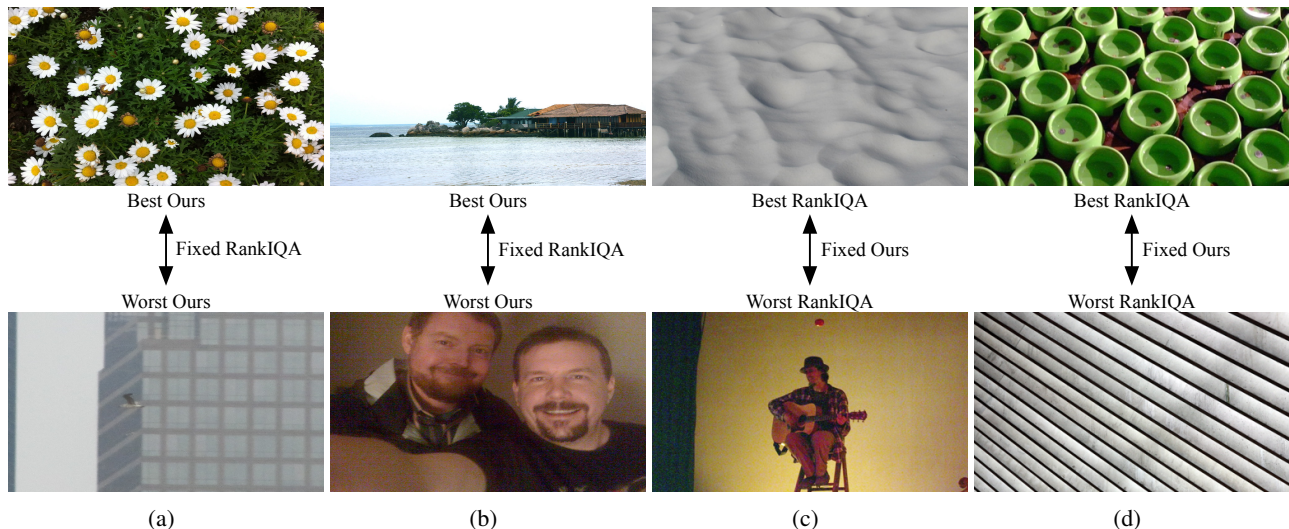


Fig. 9: Representative gMAD pairs between ours and RankIQa [20] when  $\mathcal{X}_t$  is SPAQ [6]. (a) Fixing RankIQa at the low quality level. (b) Fixing RankIQa at the high quality level. (c) Fixing ours at the low quality level. (d) Fixing ours at the high quality level.

### C. Experimental Details

The specification of feature extractor  $F$ , quality predictor  $Q$ , domain discriminator  $D$ , and the consensus learning classifier  $C$  is illustrated in Fig. 5. The backbone of the feature extractor  $F$  used in our experiment is ResNet-18 [11]. The quality predictor  $Q$  consists of three fully-connected layers and takes Leaky RELU as the activation function. The outputs of  $Q$  are two predicted values - image quality  $f_{w_q}(x)$  and corresponding STD  $\sigma_{w_q}(x)$  for an input  $x$ . To constrain the STD  $\sigma_{w_q}(x)$  to be positive, a softplus function is applied on  $\sigma_{w_q}(x)$ . Similarly, the domain discriminator and CLC are also composed using three fully-connected layers while taking RELU nonlinearity as activation function with one output representing domain label and the other for the ranking consensus, respectively.

During training,  $\lambda_1$ ,  $\lambda_2$  and  $\lambda_3$  were set to 0.08, 0.08 and 0.02 respectively, which are consistent across all the experiments. We firstly pre-trained  $F$  and  $Q$  for  $T_1 = 8$  epochs, and then performed domain adaptation  $T_2 = 2$  extra epochs. The initial learning rate was set to  $10^{-4}$  with a decay rate of 3 for every three epochs, while the learning rate of domain adaptation was set to  $10^{-6}$  remaining unchanged. Images were re-scaled and cropped into the size:  $384 \times 384 \times 3$  and served as inputs during training, while the model was tested on images of full size. Codes were written using PyTorch, and the experiments were conducted using a single NVIDIA Titan V100 GPU.



TABLE III: Summary of the learned values of hit rate  $\alpha$  and correct rejection rate  $\beta$  of each FR-IQA agents.

$\alpha$	FSIM <sub>c</sub> [63]	SR-SIM [60]	NLPD [15]	VSI [61]	MDSI [33]	GMSD [57]
Ours(naïve)	0.697	0.700	0.699	0.581	0.703	0.659
Ours(KonIQ-10k [12])	0.700	0.703	0.703	0.585	0.706	0.663
Ours(SPAQ [6])	0.700	0.703	0.703	0.585	0.706	0.663
$\beta$	FSIM <sub>c</sub>	SR-SIM	NLPD	VSI	MDSI	GMSD
Ours(naïve)	0.640	0.676	0.681	0.686	0.720	0.759
Ours(KonIQ-10k)	0.643	0.681	0.685	0.689	0.723	0.762
Ours(SPAQ)	0.643	0.681	0.685	0.689	0.723	0.762

TABLE IV: Effect of distortion mixture: results of simulating  $\mathcal{X}_s$  with single distortions.

SRCC	LIVE[39]	KonIQ-10k[12]	SPAQ[6]
Ours(KonIQ-10k)	0.905	0.640	0.753
Ours(SPAQ)	0.912	0.631	0.749
PLCC	LIVE	KonIQ-10k	SPAQ
Ours(KonIQ-10k)	0.900	0.676	0.760
Ours(SPAQ)	0.910	0.672	0.756

#### D. Evaluation Criteria

Two evaluation metrics are used to quantitatively evaluate the performance of IQA methods, *i.e.*, the Spearman’s rank correlation coefficient (SRCC) and the Pearson linear correlation coefficient (PLCC). SRCC measures the prediction monotonicity, while PLCC measures the prediction precision between MOSs and the predicted quality scores. As suggested in [48], a pre-processing step is added to linearize model predictions by fitting a four-parameter monotonic function before computing PLCC

$$\hat{f}_{w_q}(x) = (\eta_1 - \eta_2)/(1 + \exp(-(f_{w_q}(x) - \eta_3)/|\eta_4|)) + \eta_2. \quad (14)$$

where  $\{\eta_i; i = 1, 2, 3, 4\}$  are the regression parameters to be fitted.

To evaluate the generalizability and robustness of our proposed method, we also utilized group MAXimum Differentiation (gMAD) competition [26], [21], [65], [67], a widely adopted strategy for benchmarking IQA models on large-scale unlabeled datasets without human ratings. Intuitively, gMAD competition focuses on the pair of images that can falsify perceptual models in the most efficient way. Given two models, gMAD seeks a pair of images with similar quality scores predicted by one model while being assessed substantially differently by the competing model. By comparing the selected image pairs, we can easily observe the differences between two models in the error-spotting capacity, qualitatively indicating the generalizability and robustness when they work in a real-world application.

#### E. Results

1) *Quantitative comparisons*: Our proposed method was compared to six state-of-the-art *opinion-free* BIQA methods - QAC [56], NIQE [30], ILNIQE [62], RankIQA [20], dipIQ [23]

and Ma19 [25], where the first three models are knowledge-driven methods while the other three are data-driven methods. For those competing models, we used the publicly available default implementations provided by the corresponding authors for a fair comparison. TABLE II summarizes the comparison results in terms of correlation (SRCC and PLCC), where Ours( $\mathcal{X}_t$ ) with different  $\mathcal{X}_t$  indicates our methods being adapted to different target domain, *e.g.* Ours (SPQA) refers to our method with SPQA being used as target domain and Ours(naïve) is for our method with no target domain (those namings are made consistent across all of the experiments). We also include the performance on a synthetic dataset - LIVE [39] as a reference to demonstrate that our models are able to handle both synthetic distortions and authentic distortions properly.

There are several observations worth noting from the results in TABLE II. First, both knowledge-driven and data-driven BIQA methods initially designed for synthetic distortions generally work poorly on authentic distortions; in particular, the QAC method catastrophically performs on the SPAQ and KonIQ-10k. It is as expected as there exists a significant distributional discrepancy between the two data distributions, and those methods considered didn’t specifically seek to tackle this problem. Second, our proposed method outperforms six competing methods on authentic distortions even if no UDA. After UDA, a more obvious difference is observed. This indicates the effectiveness of our proposed method to learn a *opinion-free* DNN-based BIQA model. Third, the performance on SPAQ is superior to that on KonIQ-10k. This phenomenon may be due to two main reasons: 1) SPAQ includes more easily-to-handle samples; 2) the distribution of  $\mathcal{X}_s$  is close to SPAQ. Through the analysis of other competing models’ performance on two datasets, we find that the first reason may be the dominant factor. Finally, whether SPAQ or KonIQ-10k works as  $\mathcal{X}_t$ , we can obtain a similar performance improvement on authentic distortions. This may be due to shared data distribution between two datasets.

As shown in Eq.(1) and Eq.(2), the hit rate  $\alpha$  and correct rejection rate  $\beta$  are the learnable parameters indicating how much the learned network trusts those agents. To exam such confidences, we show the values of  $\alpha$  and  $\beta$  of each agent leaned by our models in TABLE III. It could be observed that *rank* of the confidences of each agent is relatively stable across different models. However, for each specific agent, the value of its confidence slightly increases when using UDA compared to the case without UDA. (*e.g.*, the value of  $\alpha$  of

TABLE V: Effects of different components and their combinations in our proposed method, including BCE, ADL, CLC and Mixup. For each metric, the best two results are highlighted in boldface

SRCC	BCE	ADL	CLC	Mixup	LIVE [39]	KonIQ-10k [12]	SPAQ [6]
Ours(KonIQ-10k)	✓				<b>0.911</b>	0.659	0.825
		✓			0.906	0.670	0.825
		✓	✓		0.907	0.707	0.827
		✓	✓	✓	0.907	<b>0.717</b>	0.826
Ours(SPAQ)	✓				0.885	0.685	0.822
		✓			0.880	0.689	0.828
		✓	✓		0.906	0.702	<b>0.834</b>
		✓	✓	✓	<b>0.920</b>	<b>0.712</b>	<b>0.838</b>
PLCC	BCE	ADL	CLC	Mixup	LIVE	KonIQ-10k	SPAQ
Ours(KonIQ-10k)	✓				0.904	0.672	0.830
		✓			0.900	0.684	0.831
		✓	✓		0.903	0.726	0.836
		✓	✓	✓	<b>0.906</b>	<b>0.740</b>	0.831
Ours(SPAQ)	✓				0.872	0.707	0.825
		✓			0.869	0.709	0.832
		✓	✓		0.902	0.729	<b>0.840</b>
		✓	✓	✓	<b>0.912</b>	<b>0.736</b>	<b>0.844</b>

agent *SR-SIM* increases from 0.700 to 0.703); Although the change of confidence is small in values, we have noted that this observation is consistent for all the agents, and as a result, the performance of the whole network improves with UDA. This indicates that the introduction of domain adaption could enable the whole network to better mine the knowledge of each agent.

2) *gMAD competition*: In gMAD competition, our method first competes with the best *opinion-free* knowledge-driven method - NIQE [30], and representative gMAD pairs are shown in Fig. 6 and 7, where target domain  $\mathcal{X}_t$  are KonIQ-10k and SPAQ, respectively. From Fig. 6(a) and (b), it could be observed that the images in the first row exhibit better perceptual quality than those in the second row (in agreement with our method while in disagreement with NIQE), indicating that our method correctly attacked NIQE by finding obvious counterexamples. When NIQE served as the attacker, our method successfully survived from the attack of NIQE, and the pairs of images found by the gMAD are of similar quality according to human perception. A similar observation was obtained when NIQE attacked our method when SPAQ was used in the target domain (see Fig. 7).

Our method was further compared to RankIQA [20] using the gMAD competition. Fig. 8 shows the gMAD image pairs in the competition between RankIQA and our method adapted with KonIQ-10k as the target. Our method favored the first row images in Fig. 8(a) and (b), which is consistent with human judgments, suggesting that our methods successfully attacked RankIQA. However, RankIQA failed to penalize the top image in Fig. 8(c) and (d), which were spotted by our method. Similarly, in Fig. 9 our method successfully identified strong failures of RankIQA (see (a) and (b)), while RankIQA failed when switching their role (see Fig. 9(c) and (d)).

In a word, the proposed method, learning from synthetic

data and multiple agents adapting to real-world distorted images, is proven to be an effective *opinion-free* BIQA in the wild, obtaining the state-of-the-art performance with improved generalizability and robustness compared to other existing *opinion-free* BIQA models.

#### F. Ablation Study

A series of ablation experiments were conducted to test the effects of different components in our proposed method, *i.e.*, distortion mixture, ADL, CLC, pixel-level domain mixup, and the number of agents.

1) *Effect of distortion mixture*: Intuitively, how to simulate  $\mathcal{X}_s$  could have an impact on final performance. To investigate this, we compare the performance of using the simulation of single distortion along with the mixture of several distortion types (see IV-B). Technically, we build a control pseudo-labeled image set based on the reference image from the Waterloo Exploration Database [22], where each image was only distorted by one type of distortions alone at five levels. Other settings, such as the generation of pseudo-labels, the rule to sample image pairs, the network structure, and hyperparameters of training, were unchanged. TABLE II and TABLE IV report the quantitative comparison results with single and mixed distortions, and significant performance gains are obtained by the strategy of distortion mixture.

2) *Effect of ADL*: Binary cross-entropy (BCE) loss is one classical objective in UDA, where the easy-to-classify samples each contributes equally to each of the hard-to-classifier samples; however, in our study, we expect the hard-to-classifier examples to contribute more, *e.g.*, to increase the weights of samples with authentic distortions that are far different from authentic distortions and reduce the weights when samples are easy to classified by domain discriminator. Thus, we introduce the ADL in Eq. (9) as the objective function of the domain

TABLE VI: Effect of the number of agents.  $\mathcal{X}_t$  is included in the bracket. The top two correlations obtained by ours are highlighted in boldface

SRCC	# of agents	LIVE [39]	KonIQ-10k [12]	SPAQ [6]
Ours(KonIQ-10k)	1	0.887	0.657	0.821
	2	0.890	0.665	0.820
	4	0.908	0.682	0.822
	6	0.907	<b>0.717</b>	0.826
Ours(SPAQ)	1	0.876	0.654	0.825
	2	0.901	0.660	0.825
	4	<b>0.913</b>	0.675	<b>0.828</b>
	6	<b>0.920</b>	<b>0.712</b>	<b>0.838</b>
PLCC	# of agents	LIVE	KonIQ-10k	SPAQ
Ours(KonIQ-10k)	1	0.881	0.679	0.825
	2	0.890	0.682	0.826
	4	0.904	0.711	0.825
	6	<b>0.906</b>	<b>0.740</b>	0.831
Ours(SPAQ)	1	0.870	0.680	0.828
	2	0.898	0.676	0.826
	4	0.906	0.698	<b>0.837</b>
	6	<b>0.912</b>	<b>0.736</b>	<b>0.844</b>

classifier. TABLE V depicts the performance comparison of BCE loss and the ADL in Eq. (9). As we can see, the ADL can yield subtle and stable performance improvement.

3) *Effect of CLC*: The CLC was introduced in our model, which is different from the quality prediction task, as a complementary objective co-optimized with the quality prediction loss to help the rectification of feature extractor (see Fig. 2). We test the performance of our model, with and without CLC; results are presented in TABLE V. It can be observed that there is an obvious performance gain after the introduction of the CLC, indicating the CLC is effective in our model and could boost the performance.

4) *Effect of domain mixup*: We further test the effect of domain pixel-level mixup regularization. TABLE V shows the difference between with/without mixup-based regularization. We observe a small performance gain achieved by incorporating a mixup strategy. This gain might attribute to the fact that the mixup operation could augment more mixed instances within each domain, thus helping the model to learn meaningful internal feature representations in the latent space.

5) *Effect of the number of agents*: Last, we study the influence of the number of agents (*i.e.*, FR-IQA models). We vary the number of agents systematically with values set to 1, 2, 4, 6 and test the performance of our method. For each of the agent numbers at 1, 2, 4, we repeated the experiments by randomly selecting three different combinations of agents and report the mean values in TABLE VI. It could be observed that, in most of the cases, with the increase of the number of FR-IQA agents used, the performances on KonIQ-10k and SPAQ are improved, and the model with six agents achieved the relatively best performance. Therefore, it is possible that the

model performance could be further improved by employing more diverse and reliable FR-IQA models.

## V. CONCLUSION

Collecting large-scale human-rated IQA image datasets is prohibitively labor-expensive and costly. Existing *opinion-free* BIQA models were mainly trained and tested on synthetically-distorted images and generalize poorly to authentically-distorted images in the wild. To tackle this issue, in this work, we present a simple and yet effective *opinion-free* BIQA model to assess the quality of images captured in the wild. Our proposed method demonstrated superior performance compared to existing ones. It has a lot of practical significance, especially for building task-specific BIQA [64], where general BIQA models do not perform well and human labels are hard to collect in those tasks, *e.g.*, perceptual optimization for colorization, super-resolution, restoration, enhancement, *etc.* Our proposed method can be potentially improved by (1) incorporating more advanced FR-IQA models and UDA methods; (2) adopting ideal distortion simulation algorithms to synthesize authentic distortions.

## ACKNOWLEDGMENT

The authors would like to thank Hanwei Zhu from City University of Hong Kong, Xuelin Liu from Jiangxi University of Finance and Economics for fruitful discussions throughout the development of this work.

## REFERENCES

- [1] Sebastian Bosse, Dominique Maniry, Klaus-Robert Müller, Thomas Wiegand, and Wojciech Samek. Deep neural networks for no-reference and full-reference image quality assessment. *IEEE Transactions on Image Processing*, 27(1):206–219, 2017. 3, 5
- [2] Christopher Burges, Tal Shaked, Erin Renshaw, Ari Lazier, Matt Deeds, Nicole Hamilton, and Gregory N Hullender. Learning to rank using gradient descent. In *International Conference on Machine Learning*, pages 89–96, 2005. 2
- [3] Baoliang Chen, Haoliang Li, Hongfei Fan, and Shiqi Wang. No-reference screen content image quality assessment with unsupervised domain adaptation. *IEEE Transactions on Image Processing*, 2021. 3
- [4] Tianlong Chen, Sijia Liu, Shiyu Chang, Yu Cheng, Lisa Amini, and Zhangyang Wang. Adversarial robustness: From self-supervised pre-training to fine-tuning. In *IEEE Conference on Computer Vision and Pattern Recognition*, pages 699–708, 2020. 5
- [5] Alexandre Ciancio, Eduardo AB da Silva, Amir Said, Ramin Samadani, Pere Obrador, et al. No-reference blur assessment of digital pictures based on multifeature classifiers. *IEEE Transactions on Image Processing*, 20(1):64–75, 2010. 3
- [6] Yuming Fang, Hanwei Zhu, Yan Zeng, Kede Ma, and Zhou Wang. Perceptual quality assessment of smartphone photography. In *IEEE Conference on Computer Vision and Pattern Recognition*, pages 3677–3686, 2020. 2, 3, 6, 7, 8, 9, 10, 11, 12, 13
- [7] Yaroslav Ganin, Evgeniya Ustinova, Hana Ajakan, Pascal Germain, Hugo Larochelle, François Laviolette, Mario Marchand, and Victor Lempitsky. Domain-adversarial training of neural networks. *The Journal of Machine Learning Research*, 17(1):2096–2030, 2016. 2, 5, 6
- [8] Deepthi Ghadiyaram and Alan C Bovik. Massive online crowdsourced study of subjective and objective picture quality. *IEEE Transactions on Image Processing*, 25(1):372–387, 2015. 2, 3, 5, 8
- [9] Ian Goodfellow, Jean Pouget-Abadie, Mehdi Mirza, Bing Xu, David Warde-Farley, Sherjil Ozair, Aaron Courville, and Yoshua Bengio. Generative adversarial networks. In *Advances in Neural Information Processing Systems*, page 2672–2680, 2014. 5
- [10] Ke Gu, Guangtao Zhai, Xiaokang Yang, and Wenjun Zhang. Deep learning network for blind image quality assessment. In *IEEE International Conference on Image Processing*, pages 511–515, 2014. 1



- [11] Kaiming He, Xiangyu Zhang, Shaoqing Ren, and Jian Sun. Identity mappings in deep residual networks. In *European Conference on Computer Vision*, pages 630–645. Springer, 2016. 10
- [12] Vlad Hosu, Hanhe Lin, Tamas Sziranyi, and Dietmar Saupe. KonIQ-10k: An ecologically valid database for deep learning of blind image quality assessment. *IEEE Transactions on Image Processing*, 29:4041–4056, 2020. 1, 2, 3, 6, 7, 8, 9, 10, 11, 12, 13
- [13] Xiangfei Kong and Qingxiang Yang. No-reference image quality assessment for image auto-denoising. *International Journal of Computer Vision*, 126(5):537–549, 2018. 8
- [14] Louisa Lam and SY Suen. Application of majority voting to pattern recognition: An analysis of its behavior and performance. *IEEE Transactions on Systems, Man, and Cybernetics*, 27(5):553–568, 1997. 5
- [15] Valero Laparra, Alexander Berardino, Johannes Ballé, and Eero P Simoncelli. Perceptually optimized image rendering. *Journal of the Optical Society of America. A, Optics, image science, and vision*, 34(9):1511–1525, 2017. 9, 11
- [16] Eric Cooper Larson and Damon Michael Chandler. Most apparent distortion: Full-reference image quality assessment and the role of strategy. *Journal of Electronic Imaging*, 19(1):011006:1–011006:21, 2010. 2
- [17] Xin Li. Blind image quality assessment. In *International Conference on Image Processing*, volume 1, pages 1–4, 2002. 3
- [18] Hanhe Lin, Vlad Hosu, and Dietmar Saupe. KADID-10k: A large-scale artificially distorted IQA database. In *International Conference on Quality of Multimedia Experience*, pages 1–3, 2019. 1
- [19] Hanhe Lin, Vlad Hosu, and Dietmar Saupe. DeepFL-IQA: Weak supervision for deep IQA feature learning. *arXiv preprint arXiv:2001.08113*, 2020. 1
- [20] Xialei Liu, Joost van de Weijer, and Andrew D Bagdanov. RankIQA: Learning from rankings for no-reference image quality assessment. In *IEEE International Conference on Computer Vision*, pages 1040–1049, 2017. 1, 2, 3, 8, 10, 11, 12
- [21] Kede Ma, Zhengfang Duanmu, Zhou Wang, Qingbo Wu, Wentao Liu, Hongwei Yong, Hongliang Li, and Lei Zhang. Group maximum differentiation competition: Model comparison with few samples. *IEEE Transactions on Pattern Analysis and Machine Intelligence*, 42(4):851–864, 2020. 3, 8, 11
- [22] Kede Ma, Zhengfang Duanmu, Qingbo Wu, Zhou Wang, Hongwei Yong, Hongliang Li, and Lei Zhang. Waterloo Exploration Database: New challenges for image quality assessment models. *IEEE Transactions on Image Processing*, 26(2):1004–1016, 2016. 1, 6, 7, 8, 12
- [23] Kede Ma, Wentao Liu, Tongliang Liu, Zhou Wang, and Dacheng Tao. dipIQ: Blind image quality assessment by learning-to-rank discriminable image pairs. *IEEE Transactions on Image Processing*, 26(8):3951–3964, 2017. 1, 3, 8, 11
- [24] Kede Ma, Wentao Liu, Kai Zhang, Zhengfang Duanmu, Zhou Wang, and Wangmeng Zuo. End-to-end blind image quality assessment using deep neural networks. *IEEE Transactions on Image Processing*, 27(3):1202–1213, 2017. 1, 3
- [25] Kede Ma, Xuelin Liu, Yuming Fang, and Eero P Simoncelli. Blind image quality assessment by learning from multiple annotators. In *IEEE International Conference on Image Processing*, pages 2344–2348, 2019. 1, 2, 4, 5, 8, 9, 11
- [26] Kede Ma, Qingbo Wu, Zhou Wang, Zhengfang Duanmu, Hongwei Yong, Hongliang Li, and Lei Zhang. Group MAD competition – a new methodology to compare objective image quality models. In *IEEE Conference on Computer Vision and Pattern Recognition*, pages 1664–1673, 2016. 11
- [27] James L Mannon and David J Sakrison. The effects of a visual fidelity criterion of the encoding of images. *IEEE Transactions on Information Theory*, 20(4):525–536, 1974. 2
- [28] Anish Mittal, Anush Krishna Moorthy, and Alan Conrad Bovik. No-reference image quality assessment in the spatial domain. *IEEE Transactions on Image Processing*, 21(12):4695–4708, 2012. 1, 3
- [29] Anish Mittal, Gautam S Muralidhar, Joydeep Ghosh, and Alan C Bovik. Blind image quality assessment without human training using latent quality factors. *IEEE Signal Processing Letters*, 19(2):75–78, 2011. 3
- [30] Anish Mittal, Ravi Soundararajan, and Alan C Bovik. Making a ‘completely blind’ image quality analyzer. *IEEE Signal Processing Letters*, 20(3):209–212, Mar. 2013. 3, 8, 11, 12
- [31] Anush Krishna Moorthy and Alan Conrad Bovik. Blind image quality assessment: From natural scene statistics to perceptual quality. *IEEE Transactions on Image Processing*, 20(12):3350–3364, 2011. 3
- [32] Jiteng Mu, Weichao Qiu, Gregory D Hager, and Alan L Yuille. Learning from synthetic animals. In *IEEE Conference on Computer Vision and Pattern Recognition*, pages 12386–12395, 2020. 2
- [33] Hossein Ziaei Nafchi, Atena Shahkolaei, Rachid Hedjam, and Mohamed Cheriet. Mean deviation similarity index: Efficient and reliable full-reference image quality evaluator. *IEEE Access*, 4:5579–5590, 2016. 9, 11
- [34] Da Pan, Ping Shi, Ming Hou, Zefeng Ying, Sizhe Fu, and Yuan Zhang. Blind predicting similar quality map for image quality assessment. In *IEEE Conference on Computer Vision and Pattern Recognition*, pages 6373–6382, 2018. 1
- [35] Tianyu Pang, Kun Xu, Chao Du, Ning Chen, and Jun Zhu. Improving adversarial robustness via promoting ensemble diversity. In *International Conference on Machine Learning*, pages 4970–4979, 2019. 5
- [36] Lionel S Penrose. The elementary statistics of majority voting. *Journal of the Royal Statistical Society*, 109(1):53–57, 1946. 5
- [37] Kuniaki Saito, Yoshitaka Ushiku, Tatsuya Harada, and Kate Saenko. Strong-weak distribution alignment for adaptive object detection. In *IEEE Conference on Computer Vision and Pattern Recognition*, pages 6956–6965, 2019. 6
- [38] Hamid R Sheikh and Alan C Bovik. Image information and visual quality. *IEEE Transactions on Image Processing*, 15(2):430–444, 2006. 3
- [39] Hamid R Sheikh, Muhammad F Sabir, and Alan C Bovik. A statistical evaluation of recent full reference image quality assessment algorithms. *IEEE Transactions on Image Processing*, 15(11):3440–3451, 2006. 1, 8, 11, 12, 13
- [40] Baochen Sun and Kate Saenko. Deep COARL: Correlation alignment for deep domain adaptation. In *European Conference on Computer Vision*, pages 443–450, 2016. 2, 3
- [41] Wei Sun, Xiongkuo Min, Guangtao Zhai, and Siwei Ma. Blind quality assessment for in-the-wild images via hierarchical feature fusion and iterative mixed database training. *arXiv preprint arXiv:2105.14550*, 2021. 2
- [42] Louis L Thurstone. A law of comparative judgment. *Psychological Review*, 34(4):273–286, 1927. 5
- [43] Eric Tzeng, Judy Hoffman, Kate Saenko, and Trevor Darrell. Adversarial discriminative domain adaptation. In *IEEE Conference on Computer Vision and Pattern Recognition*, pages 7167–7176, 2017. 2, 3, 5
- [44] Eric Tzeng, Judy Hoffman, Ning Zhang, Kate Saenko, and Trevor Darrell. Deep domain confusion: Maximizing for domain invariance. *arXiv preprint arXiv:1412.3474*, 2014. 2, 3
- [45] Gul Varol, Javier Romero, Xavier Martin, Naureen Mahmood, Michael J Black, Ivan Laptev, and Cordelia Schmid. Learning from synthetic humans. In *IEEE Conference on Computer Vision and Pattern Recognition*, pages 109–117, 2017. 2
- [46] Toni Virtanen, Mikko Nuutinen, Mikko Vaahteranoksa, Pirkko Oittinen, and Jukka Häkkinen. CID2013: A database for evaluating no-reference image quality assessment algorithms. *IEEE Transactions on Image Processing*, 24(1):390–402, 2014. 3
- [47] Vassilios Vonikakis, Ramanathan Subramanian, and Stefan Winkler. Shaping datasets: Optimal data selection for specific target distributions across dimensions. In *IEEE International Conference on Image Processing*, pages 3753–3757, 2016. 8
- [48] VQEG. Final report from the video quality experts group on the validation of objective models of video quality assessment, 2000. 11
- [49] Brian A Wandell. Foundations of vision sinauer associates. *Inc. Sunderland MA*, 1995. 2
- [50] Zhou Wang and Alan C Bovik. Reduced- and no-reference image quality assessment: The natural scene statistic model approach. *IEEE Signal Processing Magazine*, 28(6):29–40, 2011. 1
- [51] Zhou Wang, Alan C Bovik, Hamid R Sheikh, and Eero P Simoncelli. Image quality assessment: From error visibility to structural similarity. *IEEE Transactions on Image Processing*, 13(4):600–612, 2004. 1, 2, 3
- [52] Zhou Wang, Eero P Simoncelli, and Alan C Bovik. Multiscale structural similarity for image quality assessment. In *The Asilomar Conference on Signals, Systems & Computers*, pages 1398–1402, 2003. 1
- [53] Jinjian Wu, Jupuo Ma, Fuhu Liang, Weisheng Dong, Guangming Shi, and Weisi Lin. End-to-end blind image quality prediction with cascaded deep neural network. *IEEE Transactions on Image Processing*, 29:7414–7426, 2020. 3, 4
- [54] Jingtao Xu, Peng Ye, Qiaohong Li, Haiqing Du, Yong Liu, and David Doermann. Blind image quality assessment based on high order statistics aggregation. *IEEE Transactions on Image Processing*, 25(9):4444–4457, 2016. 3
- [55] Minghao Xu, Jian Zhang, Bingbing Ni, Teng Li, Chengjie Wang, Qi Tian, and Wenjun Zhang. Adversarial domain adaptation with domain mixup. In *AAAI Conference on Artificial Intelligence*, volume 34, pages 6502–6509, 2020. 5, 7
- [56] Wufeng Xue, Lei Zhang, and Xuanqin Mou. Learning without human scores for blind image quality assessment. In *IEEE Conference on Computer Vision and Pattern Recognition*, pages 995–1002, 2013. 8, 11
- [57] Wufeng Xue, Lei Zhang, Xuanqin Mou, and Alan C Bovik. Gradient magnitude similarity deviation: A highly efficient perceptual image quality index. *IEEE Transactions on Image Processing*, 23(2):684–695, 2013.

- 9, 11
- [58] Peng Ye, Jayant Kumar, and David Doermann. Beyond human opinion scores: Blind image quality assessment based on synthetic scores. In *IEEE Conference on Computer Vision and Pattern Recognition*, pages 4241–4248, 2014. 2, 3, 4
  - [59] Peng Ye, Jayant Kumar, Le Kang, and David Doermann. Unsupervised feature learning framework for no-reference image quality assessment. In *IEEE Conference on Computer Vision and Pattern Recognition*, pages 1098–1105, 2012. 1, 3
  - [60] Lin Zhang and Hongyu Li. SR-SIM: A fast and high performance iqa index based on spectral residual. In *IEEE International Conference on Image Processing*, pages 1473–1476, 2012. 9, 11
  - [61] Lin Zhang, Ying Shen, and Hongyu Li. VSI: A visual saliency-induced index for perceptual image quality assessment. *IEEE Transactions on Image Processing*, 23(10):4270–4281, 2014. 1, 2, 9, 11
  - [62] Lin Zhang, Lei Zhang, and Alan C Bovik. A feature-enriched completely blind image quality evaluator. *IEEE Transactions on Image Processing*, 24(8):2579–2591, 2015. 3, 8, 11
  - [63] Lin Zhang, Lei Zhang, Xuanqin Mou, and David Zhang. FSIM: A feature similarity index for image quality assessment. *IEEE Transactions on Image Processing*, 20(8):2378–2386, 2011. 9, 11
  - [64] Wenlong Zhang, Yihao Liu, Chao Dong, and Yu Qiao. RankSRGAN: Generative adversarial networks with ranker for image super-resolution. In *IEEE International Conference on Computer Vision*, pages 3096–3105, 2019. 13
  - [65] Weixia Zhang, Kede Ma, Jia Yan, Dexiang Deng, and Zhou Wang. Blind image quality assessment using a deep bilinear convolutional neural network. *IEEE Transactions on Circuits and Systems for Video Technology*, 30(1):36–47, 2020. 1, 11
  - [66] Weixia Zhang, Kede Ma, Guangtao Zhai, and Xiaokang Yang. Learning to blindly assess image quality in the laboratory and wild. In *IEEE International Conference on Image Processing*, pages 111–115, 2020. 1, 3, 5
  - [67] Weixia Zhang, Kede Ma, Guangtao Zhai, and Xiaokang Yang. Uncertainty-aware blind image quality assessment in the laboratory and wild. *IEEE Transactions on Image Processing*, 30:3474–3486, 2021. 3, 11